Applied Catalysis B: Environmental 144 (2014) 166–173

Contents lists available at ScienceDirect

Applied Catalysis B: Environmental

journal homepage: www.elsevier.com/locate/apcatb

Core–shell structured SiC@C supported platinum electrocatalysts for direct methanol fuel cells

Jianbing Zang, Liang Dong, Yingdan Jia, Hong Pan, Zhenzhen Gao, Yanhui Wang*

State Key Laboratory of Metastable Materials Science and Technology, College of Materials Science and Engineering, Yanshan University, Qinhuangdao 066004, PR China

ARTICLE INFO

Article history:
Received 19 April 2013
Received in revised form 16 June 2013
Accepted 23 June 2013
Available online 2 July 2013

Keywords:
Nano-SiC
Graphitization
Support
Eletrocatalyst
Stability

ABSTRACT

Core–shell structured SiC@C with a nanoscale SiC core covered by a graphitic carbon shell was used as a novel support for Pt electrocatalyst in direct methanol fuel cells (DMFCs) to achieve high durability and catalytic performance. The SiC@C was prepared by graphitization of nano-SiC under a vacuum of 10^{-3} Pa at 1500 °C. The epitaxial growth carbon layer had a high conductivity and an affinity for Pt catalyst metal, while SiC core retained its high stability. Pt electrocatalysts supported on SiC@C (Pt/SiC@C) were prepared using a microwave heating method. The electrochemical results showed that the Pt/SiC@C electrocatalyst had much higher catalytic activities for methanol electro-oxidation and oxygen reduction reactions than the Pt/SiC. More significantly, the Pt/SiC@C electrocatalyst showed a greater stability in comparison to the traditional Pt/C. The superior electrocatalytic performances of Pt/SiC@C were ascribed to a high dispersion of Pt nanoparticles on the SiC@C support and a high stability of the SiC@C support in acid solution.

1. Introduction

Polymer electrolyte membrane fuel cells (PEMFCs) including direct methanol fuel cells (DMFCs) are considered to be efficient and clean power sources and developed as an alternative to conventional power sources [1–3]. DMFCs which use methanol directly without prior complex reforming, have attracted significant attention due to easy transportation and storage of the fuel, reduced system size and weight, as well as high energy efficiency. Despite successful applications of DMFCs as vehicles, generators, and portable devices, they still suffer from insufficient stability and high-cost of electrocatalysts. Currently, most commonly used electrocatalysts in PEMFCs and DMFCs are platinum (Pt) and Pt-based alloys supported on a high surface area carbon supports [4–9]. However, carbon supports are prone to be oxidized under electrochemical conditions in DMFCs. The corrosion and microstructural degradation cause the loss of activity due to electrocatalyst detachment from matrix, and even catastrophic electrode failure [10–13]. This susceptibility directly influences the durability of Pt electrocatalyst. Therefore, the development of more advanced and stable supporting material is highly desired.

In recent years, great effort has been made on non-carbon support materials, including oxides, carbides, and nitrides [14–20]. Silicon carbide (SiC), as a wide-bandgap semiconductor material, has widespread applications in various fields, such as high-power electronic devices, ceramic reinforcement, and as substrates for synthesis of epitaxial graphene [21]. As a covalent crystal, SiC possesses many desirable properties, including high mechanical strength, thermal conductivity, and stability in acidic and oxidative environments. Besides them, nano cubic SiC with a high surface area, a large amount of surface defects and groups would exhibits better conductivity than single crystalline SiC [22], so nano-SiC is evaluated as a candidate support material for electrocatalysts in DMFCs [23–25]. However, an insufficient electrical conductivity of nano-SiC is a major obstacle for its direct use in fuel cells. Improved electrical conductivity can be achieved by incorporation of carbon black in the Pt electrocatalysts [24,26], for example, Lv et al. [24] prepared nano-SiC supported Pt electrocatalysts with high electrochemical stability and electrocatalytic performance by addition of carbon. Nonetheless, the addition of carbon black would block the active sites on the catalytic surface and hence result in low catalytic activity. Moreover, the oxidation of carbon black would result in the loss of conductivity and then the fast degradation of catalytic performance [27].

In this paper, we produced a graphitic carbon shell on nano-SiC particles using a vacuum annealing treatment. Surface graphitization resulted in epitaxial growth of carbon layer on SiC and formation of a core–shell structured SiC@C composite, which has an improved conductivity and retains high thermal and chemical stabilities in comparison to SiC. The carbon shell not only enhances the stability of Pt particles deposited on the support due to its high affinity with Pt catalyst metal, but also lowers the Ohmic contact

* Corresponding author. Tel.: +86 13780373375; fax: +86 335 8387679.
E-mail address: diamond_wangyanhui@163.com (Y. Wang).

0926-3373/$ – see front matter © 2013 Elsevier B.V. All rights reserved.
http://dx.doi.org/10.1016/j.apcatb.2013.06.031

resistivity of Pt contacts to SiC support [28], which can accelerate electron transfer in the catalyst layer. Therefore, the SiC@C composite is hopeful to be an ideal catalyst support for Pt electrocatalyst in DMFCs.

Pt electrocatalysts supported on SiC@C (Pt/SiC@C) were prepared using a microwave-assisted reduction method. The electrocatalytic effects of the prepared Pt/SiC@C electrocatalysts for anodic methanol oxidation reaction (MOR) and cathodic oxygen reduction reaction (ORR) were investigated. The stability of Pt electrocatalysts was evaluated by accelerated durability test (ADT).

2. Experimental

2.1. Chemicals

Nanocrystalline 3C-SiC powder with an average particle size of 60 nm was purchased from Hefei Kaier Nano-Power Technology Inc., China. Chloroplatinic acid ($H_2PtCl_6{\cdot}6H_2O$), methanol (CH_3OH), ethylene glycol (EG), and sulfuric acid (H_2SO_4) were purchased from Shanghai Chemical Products Ltd. Deionized water and high-purity nitrogen gas were used throughout the experiments.

2.2. Preparation and characterization of SiC@C composite

Vacuum annealing was carried out in a vacuum furnace. The nano-SiC powders were heated up to 1500 °C for 1–2 h in 10^{-3} Pa vacuum, then cooled down to ambient temperature and drawn from the vacuum furnace to atmospheric air. Raman analysis and transmission electron microscopy (TEM) were carried out before and after the annealing process. Raman analysis was performed by a Renishaw inVia Raman microscope using the 514 nm line from an Ar ion laser. The morphology was observed with a Hitachi H2120 transmission electron microscope at 200 kV and a spatial resolution of 0.2 nm.

2.3. Preparation and characterization of the electrocatalyst

Pt electrocatalysts supported on SiC@C were prepared by a microwave heating polyol method. The EG with high dielectric constant (41.4 at 298 K) and dielectric loss is rapidly heated under microwave irradiation, and then decomposed to yield CH_3CHO, which acts as a reducing agent to reduce the $(PtCl_6)^{2-}$ ion to Pt metal [29]. The reaction mechanism is described as the following equations [30].

$$CH_2OHCH_2OH = CH_3CHO + H_2O$$

$$2CH_3CHO + (PtCl_6)^{2-} = 2CH_3CHOO^- + Pt + Cl^- + 4H_2O$$

In a typical procedure, SiC@C powder of 20 mg, 0.5 mL H_2PtCl_6 (0.05 M) solution and 25 mL EG were uniformly mixed in a beaker. The beaker was placed in the center of a microwave oven (Galanz G80F23CN3XL, 2450 MHz) and heated for 80 s at 800 W. The resulting suspension was filtered and the residue was washed with acetone and deionized water. The solid products were dried at 100 °C for 12 h in a vacuum oven. For comparison, Pt electrocatalysts supported on untreated nano-SiC (Pt/SiC) and commercial carbon Vulcan XC-72 (Pt/C) were also prepared using the same process.

The crystalline structures of the prepared Pt/SiC@C were determined by means of X-ray diffraction (XRD). The measurements were carried out using a D/Max-2500pc diffractometer equipped with a standard Cu-Ka radiation source. The morphology and microstructure of the electrocatalysts were investigated by using a Hitachi H2120 transmission electron microscope. The Pt contents in the prepared electrocatalysts were determined by energy dispersion X-ray spectroscopy (EDS) on Hitachi S4800 scanning electron microscope.

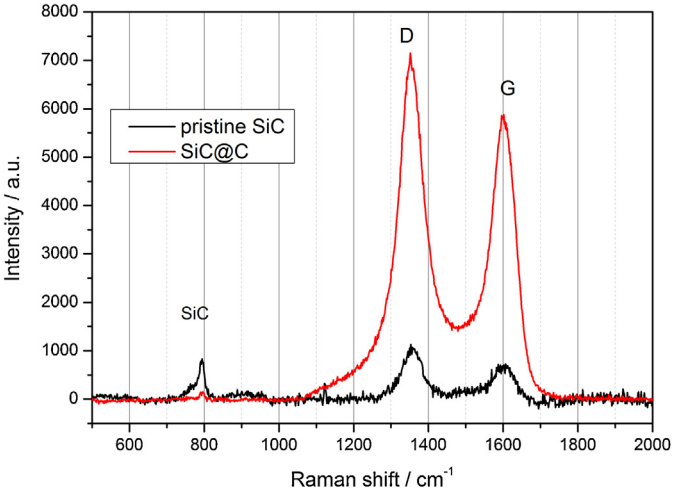

Fig. 1. Raman spectra of pristine nano-SiC and SiC@C.

2.4. Electrochemical measurements

All electrochemical measurements were carried out on a CHI660A electrochemical workstation. A conventional three-electrode system was used, consisting of a Pt electrocatalyst modified glass carbon (GC) electrode as a working electrode, a Pt coil as a counter electrode, and an Ag/AgCl electrode as a reference electrode. The working electrode was prepared as follows: the prepared electrocatalyst powder was mixed with distilled water and Nafion (20% Nafion and 80% ethanol) solution under sonicate for 20 min. One drop of the slurry (10 μL) was dropped on a GC electrode (3 mm in diameter), and then dried at 80 °C. Cyclic voltammograms (CVs) were recorded in N_2-saturated 0.5 M H_2SO_4 and 0.5 M H_2SO_4 + 1.0 M methanol solutions. Chronoamperometry (CA) curves were tested in 1.0 M methanol + 0.5 M H_2SO_4 solution at 0.4 V. The catalytic activity of the electrocatalyst toward ORR was investigated by using rotating disk electrode technique in an O_2-saturated 0.5 M H_2SO_4 solution. Linear sweeping voltammogram (LSV) was measured at different rotating speeds and a scan rate of 10 mV s^{-1}. ADT was conducted by potential sweeps from −0.2 to 1.2 V (vs. Ag/AgCl) for 800 cycles at a rate of 50 mV s^{-1} in N_2-saturated 0.5 M H_2SO_4 solution.

3. Results and discussion

3.1. Characteristics of SiC@C composite

Raman spectra were performed to investigate the surface graphitic structure of nano-SiC before and after vacuum annealing, as shown in Fig. 1. For the pristine SiC, a peak located at 791 cm^{-1} can be assigned to transverse optical phonon mode, while a wide and weak peak at 957 cm^{-1} can be ascribed to longitudinal optical phonon mode of SiC [31]. The peaks around 1597 and 1351 cm^{-1} associated with the graphitic G and D band, respectively, indicative of some graphite-like sp^2 bonded carbon [32]. After vacuum annealing at 1500 °C, the intensities of G and D peaks distinctly increased, while the peaks of SiC almost disappeared. This suggested that a surface graphitic carbon layer was thickened when the sample was annealed in vacuum. High intensity of the D band indicated a disordered graphite structure.

The further information was from TEM observation. Fig. 2 shows the TEM and high-resolution TEM (HRTEM) images of

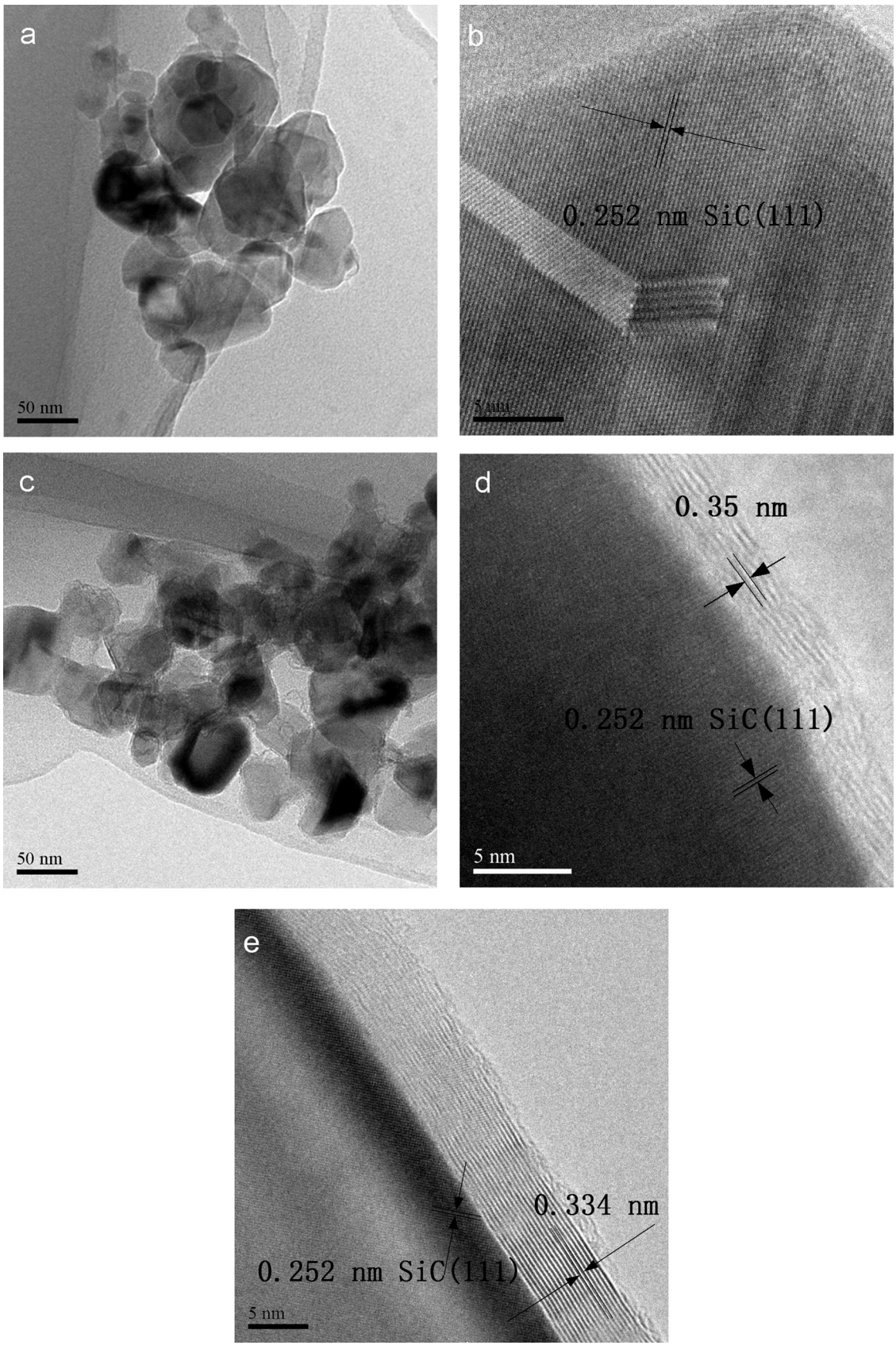

Fig. 2. TEM and HRTEM images of the pristine nano-SiC (a), (b) and SiC@C (c)–(e) powders.

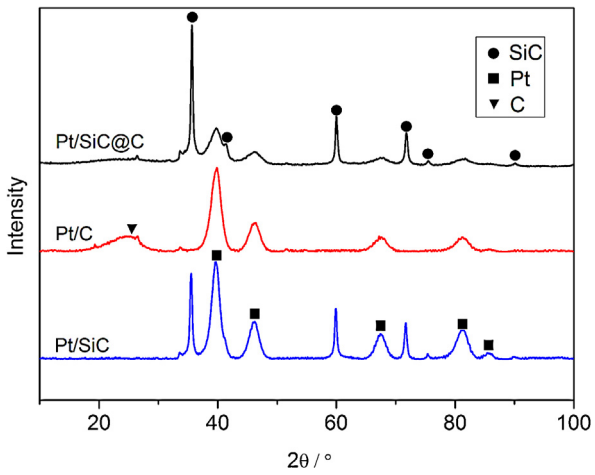

Fig. 3. XRD patterns of Pt/SiC (a), Pt/SiC@C (b), and Pt/C (c) electrocatalysts.

pristine nano-SiC (a, b) and vacuum annealing nano-SiC (c, d) powders. The pristine nano-SiC presented sphere-like particles with an average size of 60 nm (Fig. 2(a)). The HRTEM image in Fig. 2(b) indicated a crystal structure with 0.252 nm lattice fringes, which was corresponded to the (1 1 1) planes of 3C-SiC. Defects as twin crystal were clearly seen and a very thin and disconnected amorphous carbon layer presented on the surface of SiC crystal, which is consistent with the Raman analysis (Fig. 1). When SiC crystals were annealed in vacuum at 1500 °C, a core–shell structural SiC@C with a continuous graphite layer covered SiC core was obtained (Fig. 2(c)). It is well known that Si sublimation from the SiC substrate enabled a carbon enrichment of the surface [33,34]. Some turbostratic carbon layers with an interlayer distance of ~0.35 nm were observed from the HRTEM image in Fig. 2(d). The enlarged d_{002} spacing and imperfect graphenic lamellae indicated a poorly crystalline structure of the carbon shell. As annealing time prolonged, the graphitization progressed, forming planar graphite sheets with an interplanar lattice parameter of 0.334 nm (Fig. 2(e)).

3.2. Characteristics of Pt/SiC@C

Nano-SiC, SiC@C and Vulcan XC-72 carbon black supported 20 wt% Pt electrocatalysts were prepared by microwave-assisted reduction. EDS measurements confirmed that the Pt contents in the three electrocatalysts ranged from 18.4 wt% to 21.2 wt%, which agreed with the weight ratio of Pt (19.8 wt%) to support powder in the starting mixture. This indicated that almost all of Pt particles were deposited on the supports. The XRD patterns of Pt/SiC,

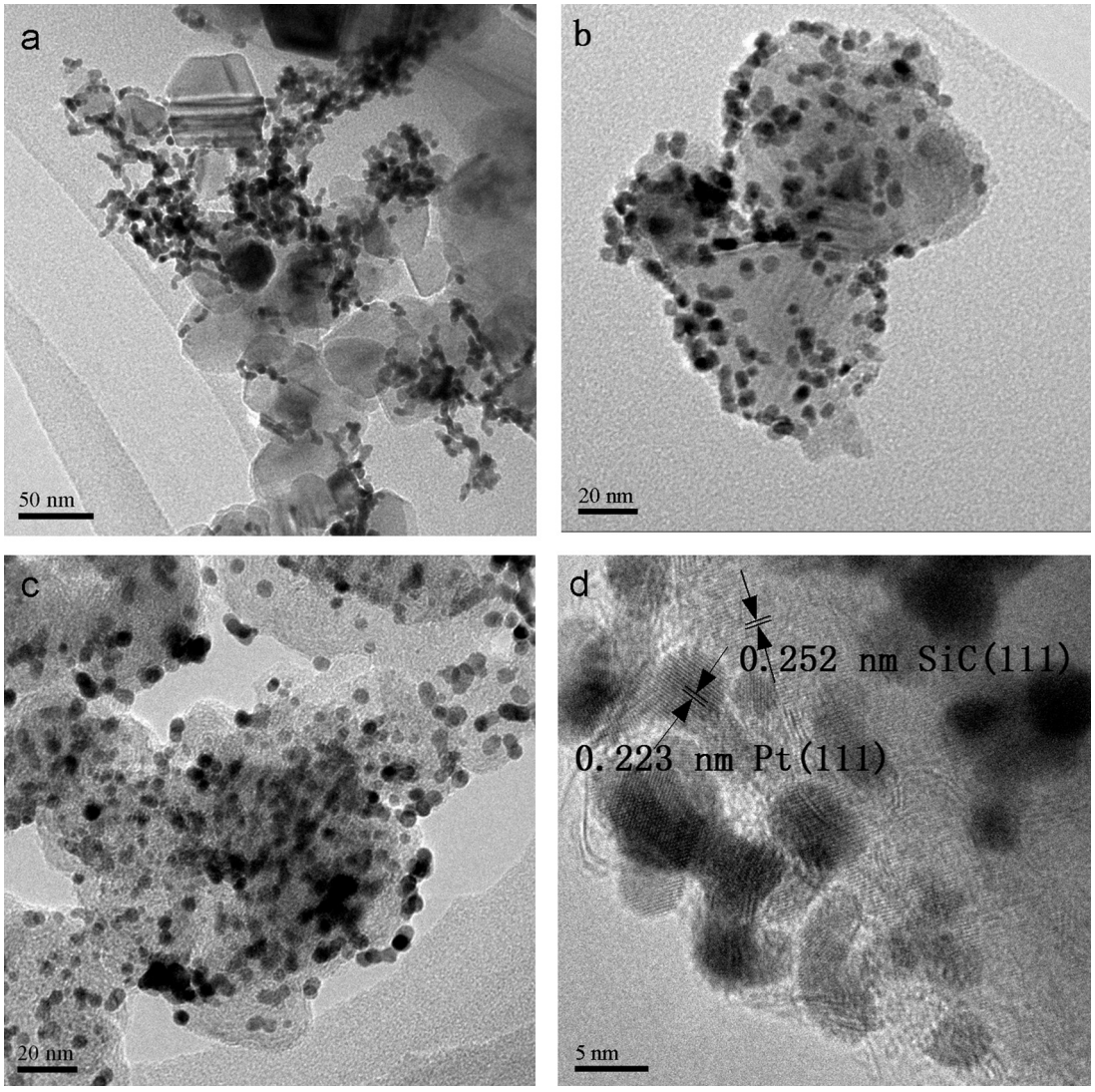

Fig. 4. TEM images of Pt/SiC (a), Pt/SiC@C (b), and Pt/C (c) electrocatalysts. (d) HRTEM image of Pt/SiC@C.

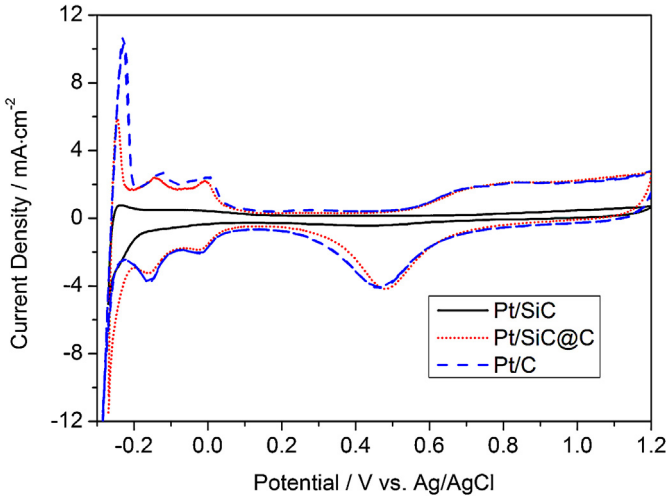

Fig. 5. CVs of Pt/SiC@C, Pt/SiC and Pt/C electrocatalysts in 0.5 M H_2SO_4, scan rate: 50 mV s^{-1}. Identical Pt electrode loading of 0.1 mg cm^{-2} was utilized for each electrode.

Pt/SiC@C and Pt/C are shown in Fig. 3. The peaks appeared at 35.52°, 41.35°, 59.88°, 71.77°, 75.48° and 89.80° correspond to the (1 1 1), (2 0 0), (2 2 0), (3 1 1), (2 2 2) and (4 0 0) planes of 3C-SiC. The characteristic peaks of Pt f.c.c crystal structure present at 39.7°, 46.2°, 67.4°, and 81.2°, corresponding to Pt (1 1 1), (2 0 0), (2 2 0), and (3 1 1) planes, respectively. The broadening diffraction peaks indicated that Pt particles had nano-scale sizes. The Pt particle sizes calculated via Scherrer equation were 3.9, 4.5, and 5.7 nm for Pt/SiC@C, Pt/C, and Pt/SiC, respectively. The decreased Pt particle size for the Pt/SiC@C as compared to Pt/SiC suggested an enhanced interaction between Pt metal and the support due to the presence of carbon shell.

Fig. 4 shows the TEM images of Pt/SiC (a), Pt/SiC@C (b), and Pt/C (c) electrocatalysts. Pt agglomerates were clearly seen on untreated nano-SiC support (Fig. 4(a)), while more homogeneous nanoparticles dispersed on SiC@C support (Fig. 4(b)), indicating a higher affinity of the Pt metal for graphitic layer compared to SiC. The size and dispersivity of Pt nanoparticles on nano-SiC@C support were similar to those on conventional carbon support (Fig. 4(c)). A high dispersion of Pt nanoparticles ensures an excellent electrocatalytic activity and a high stability of the electrocatalyst. Fig. 4(d) shows the HRTEM image of Pt/SiC@C, in which the *d*-spacing of 0.226 nm is attributed to the Pt (1 1 1) facet.

3.3. Electrochemical properties of Pt/SiC@C electrocatalysts

The CVs of Pt/SiC@C, Pt/SiC and Pt/C electrocatalysts were recorded in 0.5 M H_2SO_4 at 50 mV s^{-1} (vs. Ag/AgCl), as shown in Fig. 5. For the Pt/SiC@C, well-defined reversible peaks in the potential range of −0.3 to +0.1 V were corresponding to the adsorption/desorption peaks of hydrogen at Pt surface. It is well known that the electrochemical active surface area (ECSA) of Pt particles can be estimated from the integrated charge in the hydrogen adsorption region of the CVs [35]. The ECSA is calculated from the following formula [29]:

$$\mathrm{ECSA}\,(m^2/gPt) = Q_H/[Q_{ref} \times \mathrm{Pt\,loading}] \quad (1)$$

in which Q_H represents the number of Pt sites available for hydrogen adsorption/desorption (mC), Q_{ref} has a corresponding value of 0.21 mC cm^{-2}, which is the charge for a monolayer adsorption of hydrogen on polycrystalline Pt. The ECSA of the Pt/SiC@C electrocatalyst has been estimated to be 108.1 m^2 g^{-1}, which was similar with the ECSA of the Pt/C because of similar Pt dispersions on the two supports. While for the Pt/SiC electrocatalysts, only very weak peaks of hydrogen adsorption/desorption can be seen, indicating a small ECSA. This should be attributed to the poor conductivity of the SiC supports [36]. The carbon shell on nano-SiC provided a high conductivity as well as an improved dispersion of Pt nanoparticles, which are prerequisites for achieving a high catalytic activity of the electrocatalysts.

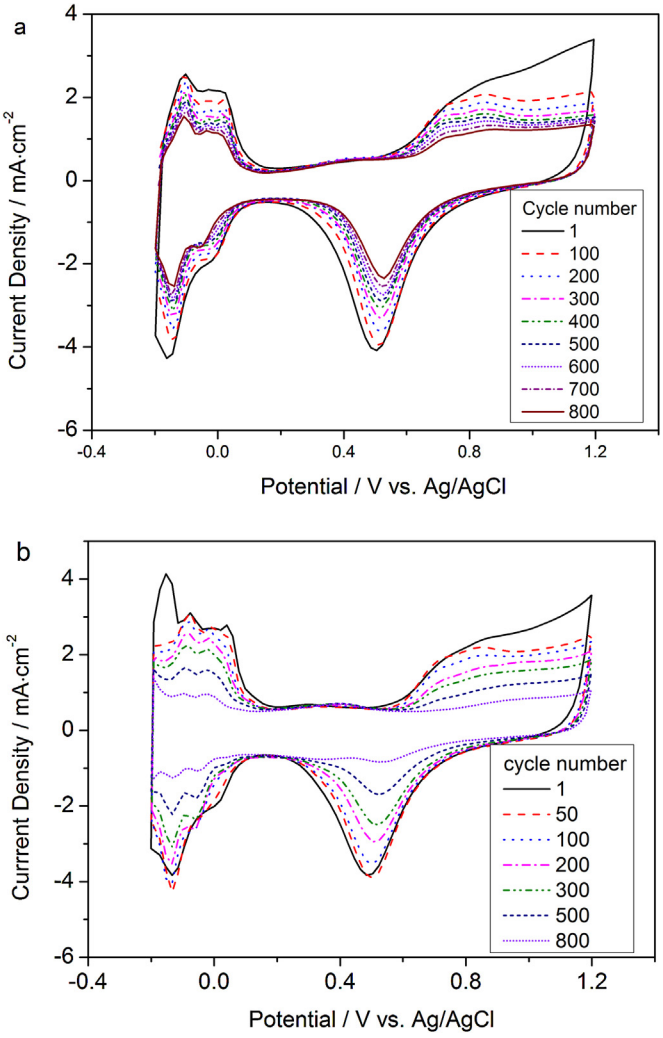

Fig. 6. CVs of the Pt/SiC@C (a) and Pt/C (b) electrocatalysts before and after 800 cycles. (c) Variations of the ECSA values with cycle number.

ADT has been conducted by continuous potential cycling from −0.2 to 1.2 V (vs. Ag/AgCl) in 0.5 M H_2SO_4 solution to evaluate the durability of the electrocatalysts. Fig. 6(a) shows the CVs of the Pt/SiC@C electrocatalysts before and after 800 cycles. For comparison, the CVs of the Pt/C electrocatalysts after cycling were also given in Fig. 6(b). The variations of the ECSA values with cycle number during the ADT were calculated from the hydrogen desorption integrals, as shown in Fig. 6(c). The ECSAs of electrocatalysts reduced with cycle number because of aggregation or dissolution of Pt nanoparticles in acid solution, which would speed up by corrosion of supports [12,37,38]. From Fig. 6(c), it was seen that the ECSA degradation rate of the Pt/SiC@C was distinctly lower than that of the Pt/C. After 800 cycles, the ECSA of the Pt/SiC@C retained 53.9%, while the traditional Pt/C has only 17.1% ECSA remained. The results showed an excellent stability of the Pt/SiC@C. The carbon supports are prone to be oxidized at high potentials (above 1.0 V vs. Ag/AgCl), and the support oxidation would promote aggregation or dissolution of Pt nanoparticles, producing a rapid decrease in ECSA. As for

the SiC@C supports, both SiC core and epitaxial graphitic shell have higher oxidation resistance compared to amorphous carbon black (Vulcan XC-72), and consequently generate a high stability for the Pt/SiC@C electrocatalysts.

The CVs of Pt/SiC@C, Pt/SiC, and Pt/C electrocatalysts in aqueous solution of 0.5 M H_2SO_4 containing 1.0 M CH_3OH were recorded at 50 mV s^{-1}, as shown in Fig. 7. The currents in Fig. 7(a) were normalized by the electroactive surface, so they can represent intrinsic activity effect of the electrocatalysts. It was seen that the methanol oxidation peak current densities both in the forward scan and the backward scan on the Pt/SiC@C were slightly higher than that on the Pt/C, and far higher than that on the Pt/SiC. The area-normalized current density at 0.4 V for Pt/SiC@C (0.07 mA cm^{-2}) was also higher in comparison with the Pt/C (0.06 mA cm^{-2}) and the Pt/SiC (0.02 mA cm^{-2}), suggesting a high electrocatalytic activity of the Pt/SiC@C for the methanol oxidation. The improved electrocatalytic performance of the Pt/SiC@C should be ascribed to an improved dispersion of Pt nanoparticles due to a strong interaction between SiC@C support and Pt nanoparticles and an increased conductivity by carbon shell. Fig. 7(b) shows CVs normalized by Pt mass on each electrode. The Pt/SiC@C had a similar mass-normalized current density (554 mA mg^{-1} Pt) with the Pt/C electrocatalyst (551 mA mg^{-1} Pt), which is much higher than that of the Pt/SiC (13 mA mg^{-1} Pt). Further information was from CA curves in Fig. 7(c), which were recorded in 1.0 M methanol + 0.5 M H_2SO_4 solution at 0.4 V. An initial rapid current decay in CA curves was possibly due to the electrocatalyst poisoning by CO-like intermediate species generated during the continuous oxidation process. In comparison with the commercial Pt/C, the Pt/SiC@C electrocatalysts exhibited similar initial current but lower rate of current decay, confirming high catalytic activity and stability for methanol oxidation as well as high CO tolerance.

Fig. 8(a) shows the LSVs for ORRs on Pt/SiC@C, Pt/SiC, and Pt/C electrocatalysts in O_2-saturated 0.5 M H_2SO_4, vs. Ag/AgCl. The onset potential for the ORR on the Pt/SiC@C electrocatalyst was much more positive than that on Pt/SiC, and comparable to Pt/C electrocatalysts. Fig. 8(b) and (c) show the LSV curves of the Pt/SiC@C and Pt/C electrocatalysts obtained at various rotation rates on RDE. The reduction current can be expressed as Koutecky–Levich equation [39,40].

$$\frac{1}{j} = \frac{1}{j_k} + \frac{1}{B\omega^{1/2}} \quad (2)$$

where j_k is the kinetically controlled current density, ω is the angular rotation frequency (rad s^{-1}), B is Levich constant. The Koutecky–Levich curves (j^{-1} vs. $\omega^{-1/2}$) plotted in insets showed a good linear dependence at various potentials. The Levich constant (B) obtained from the slope of the curves was used to be calculate the number of electrons transferred per molecule of oxygen involved in the ORR process according to Eq. (3) [39].

$$B = 0.2nFA(\mathrm{Do}_2)^{2/3}\nu - 1/6\mathrm{Co}_2 \quad (3)$$

where n is the number of electrons exchanged per molecule oxygen, F is Faraday constant, A is the surface area of the electrode, Co_2 is the molecular oxygen concentration in the electrolyte, Do_2 is the oxygen diffusion coefficient, ν is the viscosity of the electrolyte. The average number of transferred electrons for Pt/SiC@C and Pt/C were calculated as 3.80 and 3.83, respectively, indicative of a four-electron process involved in the ORR for both electrocatalysts. The mass transfer-corrected Tafel plots derived from the voltammetric data of Fig. 8(b) and (c) are presented in Fig. 8(d), whereby the kinetic current density (j_k) is given per Pt electroactive surface area. The mass transfer-corrected j_k was given from the equation:

$$j_k = \frac{j \cdot j_d}{j_d - j} \quad (4)$$

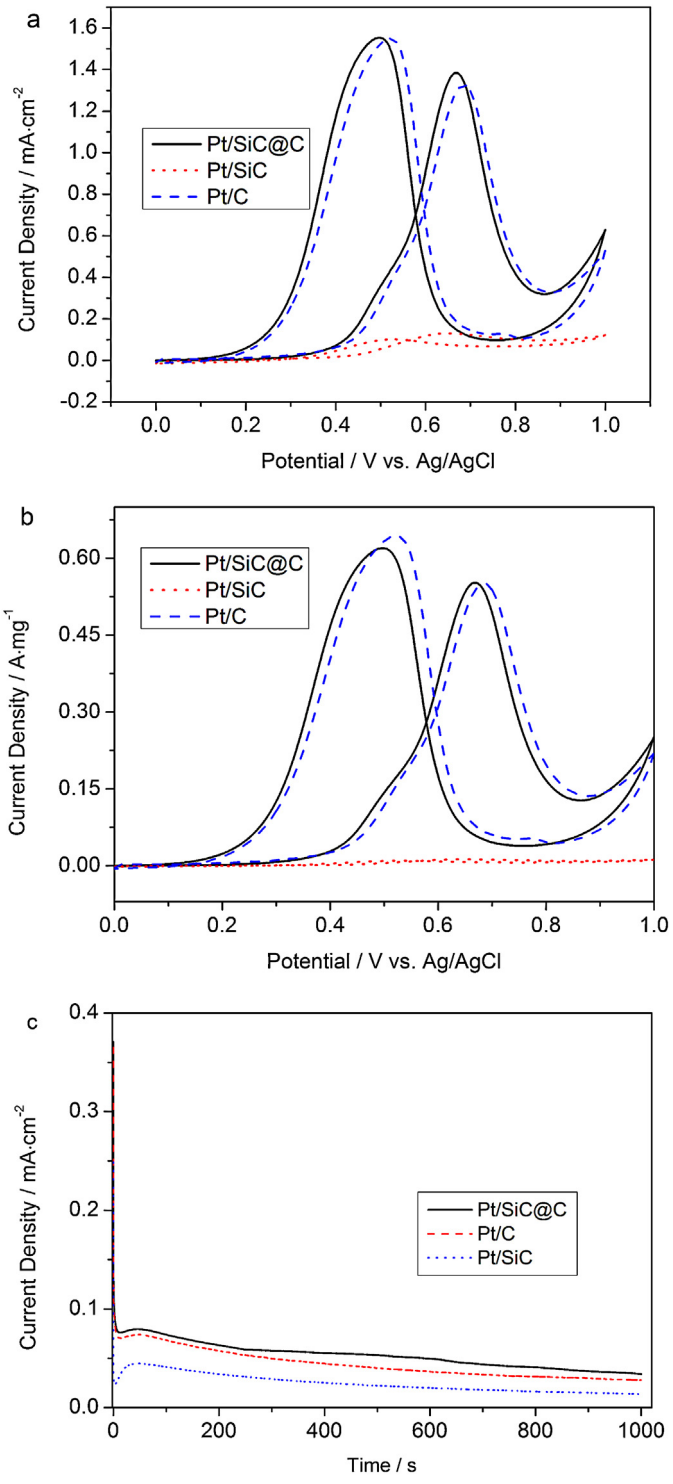

Fig. 7. CVs of Pt/SiC@C, Pt/SiC, and Pt/C electrocatalysts in 1.0 M CH_3OH + 0.5 M H_2SO_4 at a scan rate of 50 mV s^{-1}, the currents were normalized by (a) electrochemical active surface areas and (b) amount of loading of catalysts, respectively. (c) CA curves of Pt/SiC@C, Pt/SiC, and Pt/C electrocatalysts in 1.0 M CH_3OH + 0.5 M H_2SO_4 at 0.4 V.

where j is overall measured current density, j_d is diffusion limiting current density. The Tafel slopes in low current regions were estimated to be −63 and −67 mV dec^{-1} for Pt/SiC@C and Pt/C, respectively, which corresponded to oxygen reduction occurring on a high surface oxide coverage Pt electrode under Temkin oxygen adsorption conditions [41]. Both electrocatalysts presented a Tafel slope of −120 mV dec^{-1} in high current regions, indicating

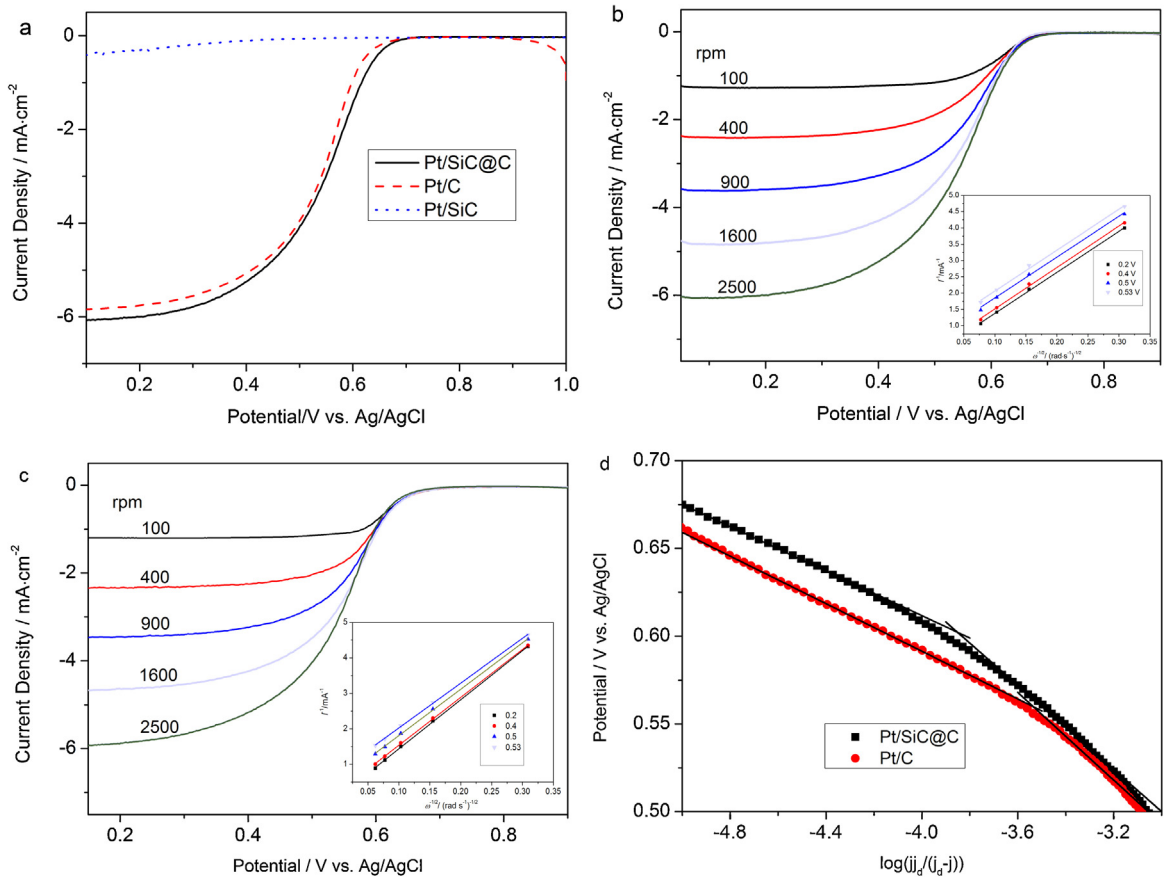

Fig. 8. (a) LSVs of Pt/SiC@C, Pt/SiC, and Pt/C electrocatalysts on RDE in O_2-saturated 0.5 M H_2SO_4. Sweep direction: negative-going. Sweep rate: 10 mV s^{-1}. Rotation rate for LSV: 2500 rpm. (b) and (c) LSVs of Pt/SiC@C, Pt/C electrocatalysts on RDE in O_2-saturated 0.5 M H_2SO_4 at different rotation rates, the insets show Koutecky–Levich curves at different potentials according to the date of (b) and (c). (d) Mass transfer-corrected Tafel plots from data of Fig. 8(b) and (c).

that the rate determining step was the transfer of the first electron to oxygen molecule with the transfer coefficient β=0.5 [41,42]. The change of the slope was attributed to the potential-dependent coverage of surface oxides that inhibit the adsorption of O_2 and reaction intermediates [43,44]. All these results showed similar or even superior catalytic performances for the Pt/SiC@C electrocatalyst compared to the Pt/C due to the unique core–shell structure of the SiC@C support.

4. Conclusions

Surface graphitization of nano-SiC was carried out by annealing nano-SiC powder in a 10^{-3} Pa vacuum at 1500 °C. A core–shell structural SiC@C with a continuous graphitic carbon layer covered a SiC core was obtained. The SiC@C had an improved conductivity and an enhanced affinity with Pt metal, while SiC core retained its high stability. The nano-SiC@C was used as a supporting material for fabrication of Pt electrocatalysts using the microwave heating method. More homogeneous Pt nanoparticles dispersed on nano-SiC@C compared to nano-SiC. The electrochemical results showed that the Pt/SiC@C electrocatalyst had much better catalytic activities for MOR and ORR than Pt/SiC. More significantly, the Pt/SiC@C electrocatalysts had greater stability in comparison to traditional Pt/C. The excellent catalytic performances can be ascribed to the unique core–shell structure of SiC@C support, in which the carbon shell provided a high conductivity and a high affinity with Pt metal, the SiC core provided a high stability in acid solution.

Acknowledgements

This work was supported by the National Natural Science Foundation of China (Nos. 51272226 and 50972125), the Natural Science Foundation of Hebei Province (Nos. E2012203112 and E2011203126).

References

[1] A.Z. Weber, J. Newman, Chem. Rev. 104 (2004) 4679–4726.
[2] Y. Shao, J. Liu, Y. Wang, Y. Lin, J. Mater. Chem. 19 (2009) 46–59.
[3] Z. Wen, J. Li, J. Mater. Chem. 19 (2009) 8707.
[4] E. Antolini, Appl. Catal. B: Environ. 88 (2009) 1–24.
[5] A. Pozio, M. De Francesco, A. Cemmi, F. Cardellini, L. Giorgi, J. Power Sources 105 (2002) 13–19.
[6] J.R.C. Salgado, R.G. Duarte, L.M. Ilharco, A.M. Botelho do Rego, A.M. Ferraria, M.G.S. Ferreira, Appl. Catal. B: Environ. 102 (2011) 496–504.
[7] D. Sebastián, A.G. Ruíz, I. Suelves, R. Moliner, M.J. Lázaro, V. Baglio, A. Stassi, A.S. Aricò, Appl. Catal. B: Environ. 115–116 (2012) 269–275.
[8] Y. Takasu, T. Kawaguchi, W. Sugimoto, Y. Murakami, Electrochim. Acta 48 (2003) 3861–3868.
[9] J. Qi, L. Jiang, S. Wang, G. Sun, Appl. Catal. B: Environ. 107 (2011) 95–103.
[10] X.-Z. Yuan, H. Li, S. Zhang, J. Martin, H. Wang, J. Power Sources 196 (2011) 9107–9116.
[11] J. Wang, G.M. Swain, J. Electrochem. Soc. 150 (2003) E24–E32.
[12] Y. Shao, G. Yin, Y. Gao, J. Power Sources 171 (2007) 558–566.
[13] K.H. Kangasniemi, D. Condit, T. Jarvi, J. Electrochem. Soc. 151 (2004) E125.
[14] S.-Y. Huang, P. Ganesan, B.N. Popov, Appl. Catal. B: Environ. 102 (2011) 71–77.
[15] S. Sharma, B.G. Pollet, J. Power Sources 208 (2012) 96–119.
[16] B. Abida, L. Chirchi, S. Baranton, T.W. Napporn, H. Kochkar, J.-M. Léger, A. Ghorbel, Appl. Catal. B: Environ. 106 (2011) 609–615.
[17] B. Avasarala, T. Murray, W. Li, P. Haldar, J. Mater. Chem. 19 (2009) 1803–1805.
[18] S. Yin, S. Mu, H. Lv, N. Cheng, M. Pan, Z. Fu, Appl. Catal. B: Environ. 93 (2010) 233–240.

[19] E. Antolini, E.R. Gonzalez, Solid State Ionics 180 (2009) 746–763.
[20] J.-M. Lee, S.-B. Kim, Y.-W. Lee, D.-Y. Kim, S.-B. Han, B. Roh, I. Hwang, K.-W. Park, Appl. Catal. B: Environ. 111–112 (2012) 200–207.
[21] M.-S. Hu, C.-C. Kuo, C.-T. Wu, C.-W. Chen, P.K. Ang, K.P. Loh, K.-H. Chen, L.-C. Chen, Carbon 49 (2011) 4911–4919.
[22] N. Yang, H. Zhuang, R. Hoffmann, W. Smirnov, J. Hees, X. Jiang, C.E. Nebel, Anal. Chem. 83 (2011) 5827–5830.
[23] X. Tong, L. Dong, G. Jin, Y. Wang, X.Y. Guo, Fuel Cells 11 (2011) 907–910.
[24] H. Lv, S. Mu, N. Cheng, M. Pan, Appl. Catal. B: Environ. 100 (2010) 190–196.
[25] L. Fang, X.-P. Huang, F.J. Vidal-Iglesias, Y.-P. Liu, X.-L. Wang, Electrochem. Commun. 13 (2011) 1309–1312.
[26] A. Honji, T. Mori, Y. Hishinuma, K. Kurita, J Electrochem. Soc. 135 (1988) 917–918.
[27] B.Y. Xia, S. Ding, H.B. Wu, X. Wang, X. Wen, RSC Adv. 2 (2012) 792–796.
[28] F. Liu, B. Hsia, C. Carraro, A. Pisano, R. Maboudian, Appl. Phys. Lett. 97 (2010) 262103–262107.
[29] W.X. Chen, J.Y. Lee, Z. Liu, Chem. Commun. (2002) 2588–2589.
[30] X. Li, W.-X. Chen, J. Zhao, W. Xing, Z.-D. Xu, Carbon 43 (2005) 2168–2174.
[31] S. Rohmfeld, M. Hundhausen, L. Ley, Phys. Rev. B 58 (1998) 9858.
[32] J. Jeong, K. Jang, H.S. Lee, G.-S. Chung, G.-y Kim, Physica B Condens. Matter 404 (2009) 7–10.
[33] A. Ouerghi, R. Belkhou, M. Marangolo, M. Silly, S. El Moussaoui, M. Eddrief, L. Largeau, M. Portail, F. Sirotti, Appl. Phys. Lett. 97 (2010) 161905.
[34] N. Gogneau, A. Balan, M. Ridene, A. Shukla, A. Ouerghi, Surf. Sci. (2011).
[35] M. Hupert, A. Muck, J. Wang, J. Stotter, Z. Cvackova, S. Haymond, Y. Show, G.M. Swain, Diam. Relat. Mater. 12 (2003) 1940–1949.
[36] Z.-Z. Jiang, Z.-B. Wang, Y.-Y. Chu, D.-M. Gu, G.-P. Yin, Energy Environ. Sci. 4 (2011) 728–735.
[37] S. Zhang, X.-Z. Yuan, J.N.C. Hin, H. Wang, K.A. Friedrich, M. Schulze, J. Power Sources 194 (2009) 588–600.
[38] J. Qi, S. Yan, Q. Jiang, Y. Liu, G. Sun, Carbon 48 (2010) 163–169.
[39] R. Wang, X. Li, H. Li, Q. Wang, H. Wang, W. Wang, J. Kang, Y. Chang, Z. Lei, Int. J. Hydrogen Energy 36 (2011) 5775–5781.
[40] Y. Wang, S. Song, V. Maragou, P.K. Shen, P. Tsiakaras, Appl. Catal. B: Environ. 89 (2009) 223–228.
[41] A. Tegou, S. Papadimitriou, E. Pavlidou, G. Kokkinidis, S. Sotiropoulos, J. Electroanal. Chem. 608 (2007) 67–77.
[42] A. Sarapuu, A. Kasikov, T. Laaksonen, K. Kontturi, K. Tammeveski, Electrochim. Acta 53 (2008) 5873–5880.
[43] J. Wang, N. Markovic, R. Adzic, J. Phys. Chem. B 108 (2004) 4127–4133.
[44] J.X. Wang, F.A. Uribe, T.E. Springer, J. Zhang, R.R. Adzic, Faraday Discuss. 140 (2009) 347–362.